

# Journal of Fluid Mechanics

<http://journals.cambridge.org/FLM>

Additional services for *Journal of Fluid Mechanics*:

Email alerts: [Click here](#)

Subscriptions: [Click here](#)

Commercial reprints: [Click here](#)

Terms of use : [Click here](#)



---

## Planar flows past thin multi-blade configurations

F. T. Smith and S. N. Timoshin

Journal of Fluid Mechanics / Volume 324 / October 1996, pp 355 - 377

DOI: 10.1017/S0022112096007951, Published online: 26 April 2006

**Link to this article:** [http://journals.cambridge.org/abstract\\_S0022112096007951](http://journals.cambridge.org/abstract_S0022112096007951)

### How to cite this article:

F. T. Smith and S. N. Timoshin (1996). Planar flows past thin multi-blade configurations. Journal of Fluid Mechanics, 324, pp 355-377 doi:10.1017/S0022112096007951

**Request Permissions :** [Click here](#)

# Planar flows past thin multi-blade configurations

By F. T. SMITH AND S. N. TIMOSHIN

Mathematics Department, University College, Gower St., London, WC1E 6BT, UK

(Received 16 October 1995 and in revised form 6 March 1996)

Two-dimensional steady laminar flows past multiple thin blades positioned in near or exact sequence are examined for large Reynolds numbers. Symmetric configurations require solution of the boundary-layer equations alone, in parabolic fashion, over the successive blades. Non-symmetric configurations in contrast yield a new global inner–outer interaction in which the boundary layers, the wakes and the potential flow outside have to be determined together, to satisfy pressure-continuity conditions along each successive gap or wake. A robust computational scheme is used to obtain numerical solutions in direct or design mode, followed by analysis. Among other extremes, many-blade analysis shows a double viscous structure downstream with two streamwise length scales operating there. Lift and drag are also considered. Another new global interaction is found further downstream. All the interactions involved seem peculiar to multi-blade flows.

---

## 1. Introduction

Fluid flows past thin multiple blades or airfoils are of practical as well as theoretical interest in both two-dimensional and three-dimensional motion. Of special interest are flows where successive airfoil–wake, blade–wake or blade–vortex interactions occur, in an approximately streamlined configuration of blades positioned in sequence. Many practical applications in three-dimensional rotary flows are considered by Smith & Timoshin (1996), including rotorcraft, propellers, fans, mixers, blenders, hover mowers and so on. To these may be added non-rotary applications of multi-airfoils or multi-blades, such as in the use of trailing-edge or leading-edge flaps, pursuit problems, delay problems, for example concerning take-off or landing at busy airfields (see also Moore & Saffman 1973), and related issues of slip-streaming. The number of blades or airfoils involved varies from few to many, depending on the specific context. There are certain significant issues which are common to most contexts, nevertheless, for example regarding the influence of vorticity shedding from one blade to another, the quantitative amount of sheltering felt by successive blades, in terms of drag or velocity reduction just ahead of each blade, the induced lift and drag, downstream wake properties, and the benefits and disadvantages inherent in these motions.

The current study for high Reynolds numbers is based on Smith & Timoshin's (1996) approach addressing three-dimensional boundary layers on rotary blades. They present an alternative view of blade–wake interactions based on the three-dimensional rotary boundary-layer equations as distinct from many previous inviscid approaches, e.g. see Davis & Chang (1986), Seddon (1990), Wake & Baeder (1994) for recent reviews and see inviscid sheltering effects in Glauert (1948) concerning staggered or in-tandem or rotating blades. Several new types of interaction are also identified in Smith & Timoshin. The latter paper is restricted to a symmetric regime corresponding to a

hovering type of rotary motion with zero lift, but some discussion is given comparing non-symmetric and symmetric situations, in addition to steady and unsteady, two-dimensional and three-dimensional situations, all of which have their own special attributes. The present investigation is mostly on two-dimensional steady models, in particular tackling aspects of non-symmetry as well as symmetry, although connected features of three-dimensional flows and of unsteadiness are also to be described. This is for blades and wakes in an otherwise uniform stream, the positioning of the blades being exactly or approximately sequential, such that significant intersections of wakes with blades continue downstream; similar considerations may be applied to in-parallel positionings for instance. The presence of non-symmetry enables lifting multi-blade flows to be examined, in this simpler two-dimensional context, with the hope of providing helpful ideas for the treatment of lifting three-dimensional cases subsequently; one close link between the two-dimensional and the three-dimensional cases is actually seen to emerge in a limiting situation later in this paper. The promises of application to realistic three-dimensional flows and to unsteady or transitional motions, coupled with the new questions that are found to arise, motivate the theoretical and computational research described below.

With non-symmetry present, inner-outer interaction enters as a major fresh feature, anticipated in the last paper. The inner boundary-layer (and wake) flow properties and the outer potential-flow disturbances must be determined simultaneously, in order to satisfy continuity of pressure across each wake. In particular the wake centreline curves and the starting velocity profiles for the boundary layers are unknown in advance generally. Moreover this inner-outer interaction is global, extending over the entirety of each blade and wake, unlike most other interactions such as triple deck and double deck which are local instead. Here we should stress that as in the last paper our concern is with laminar motions to start matters, to be followed later by aspects of transition. In addition to the onset of interactions here the flow responses are inherently nonlinear, in essence because of all the leading and trailing edges active within the boundary layers and wakes. These edges in turn require a flexible robust numerical treatment to be used. Non-symmetry drives the inner nonlinear system coupled with the outer linear system, making the overall interaction become elliptic in effect and the task much more complex than in the symmetric situation where interaction is absent. The fundamental cases addressed in this work have the blade thicknesses, cambers and angles of incidence all being small, comparable with the non-dimensional boundary-layer and wake thicknesses, and producing separation-free flows, in order to clarify the nonlinear inner-outer interaction(s) present.

Section 2 below first describes the main two-dimensional cases studied, (a) symmetric flows (§2.1) and (b) non-symmetric flows (§2.2), and then links them with (c) three-dimensional rotary motions (§2.3). Case (a) is covered by the two-dimensional boundary-layer equations in a parabolic manner, as addressed in §3, while (b) couples those equations elliptically with the outer potential-flow equations as considered in §4. Analytical and computational properties are described, the computations being either of direct or of inverse/design type. A number of interesting properties seem to arise. For example, if there are many blades (cf. Hawkings & Lowson 1974; Parry & Crighton 1989 in inviscid theory on rotor acoustics) a doubly viscous flow structure emerges downstream with two associated streamwise length scales also operating, for both cases (a) and (b). It is perhaps surprising then to find that the Blasius solution always remains relevant downstream, in a mean sense, even for instance when each blade chord is extremely (asymptotically) short compared with each wake length in some circumstances. The latter may apply to certain helicopter blade motions, given

the suggestion from Smith & Timoshin's results that many-blade analysis works reasonably well for moderately large numbers of blades. Section 5 considers the lift and drag produced, while further comments are given briefly in §6, including yet another new kind of inner-outer interaction which again affects the whole of each blade and wake but which raises the prospect of regular separations being induced on successive blades. This last interaction which has many applications (§6) should allow increased rational understanding of multiple separations in these flows, unlike in inviscid theory, and, further, the interaction and its predecessor in §4 seem to be the first to cover entire blades or airfoils in a rational fashion, with or without separations occurring.

The non-dimensional Cartesian coordinates  $(x, y)$  (streamwise and normal respectively), corresponding velocity components  $(u, v)$  and pressure  $p$  used below are based on  $\ell_D, u_D, \rho_D u_D^2$  in turn, where  $\ell_D$  is the typical airfoil or blade chord,  $u_D$  is the incident free-stream velocity, and  $\rho_D$  is the density of the incompressible fluid. The free-stream pressure is taken as zero. The characteristic global Reynolds number  $Re \equiv u_D \ell_D \nu_D^{-1}$  is large, where  $\nu_D$  is the kinematic viscosity of the fluid, and so the typical boundary-layer and wake thicknesses are of order  $Re^{-1/2}$ , as are the blade thicknesses, cambers and angles of incidence in the present setting. The number of blades is  $n(\geq 1)$ .

## 2. Two-dimensional multi-blade flows; and relevance to three-dimensional rotary multi-blade flows

Here we pose first the two-dimensional multiple blade problems ((a) symmetric, (b) non-symmetric) that form the core of our subsequent investigation and then (in (c)) discuss their relevance to the three-dimensional multiple-blade issues raised in Smith & Timoshin (1996).

### 2.1. Two-dimensional motions, symmetric

In this simplest configuration a sequence of thin symmetric blades or airfoils is situated parallel to the uniform stream, in a 'slip-streaming' arrangement with each leading and trailing edge lying on the  $x$ -axis, the first being at the origin. See figure 1(a). The number of blades,  $n$ , may be finite or infinite, but their thicknesses are such as to avoid leading- or trailing-edge separations. Specifically we will tend to consider mostly  $O(Re^{-1/2})$  thicknesses later and so we may as well do so now, taking the blade shapes to be given by  $y = Re^{-1/2}f(x)$ , say, where  $f$  is smooth and  $O(1)$  typically and vanishes at each leading and trailing edge.

The aim in this case is basically to resolve the viscous boundary-layer and wake motions for all the blades. The motions, which are supposed to be symmetric in  $y$ , are controlled by the boundary-layer equations for the scaled velocity components  $u, V \{ \equiv Re^{1/2}v - uf'(x) \}$ ,

$$u_x + V_Y = 0, \quad (2.1a)$$

$$uu_x + Vu_Y = 0 + u_{YY}, \quad (2.1b)$$

subject to the no-slip, wake-symmetry and free-stream conditions

$$u = V = 0 \text{ at } Y = 0 \text{ on each blade,} \quad (2.1c)$$

$$u_Y = V = 0 \text{ at } Y = 0 \text{ in each wake,} \quad (2.1d)$$

$$u \rightarrow 1 \text{ as } Y \rightarrow \infty, \quad (2.1e)$$

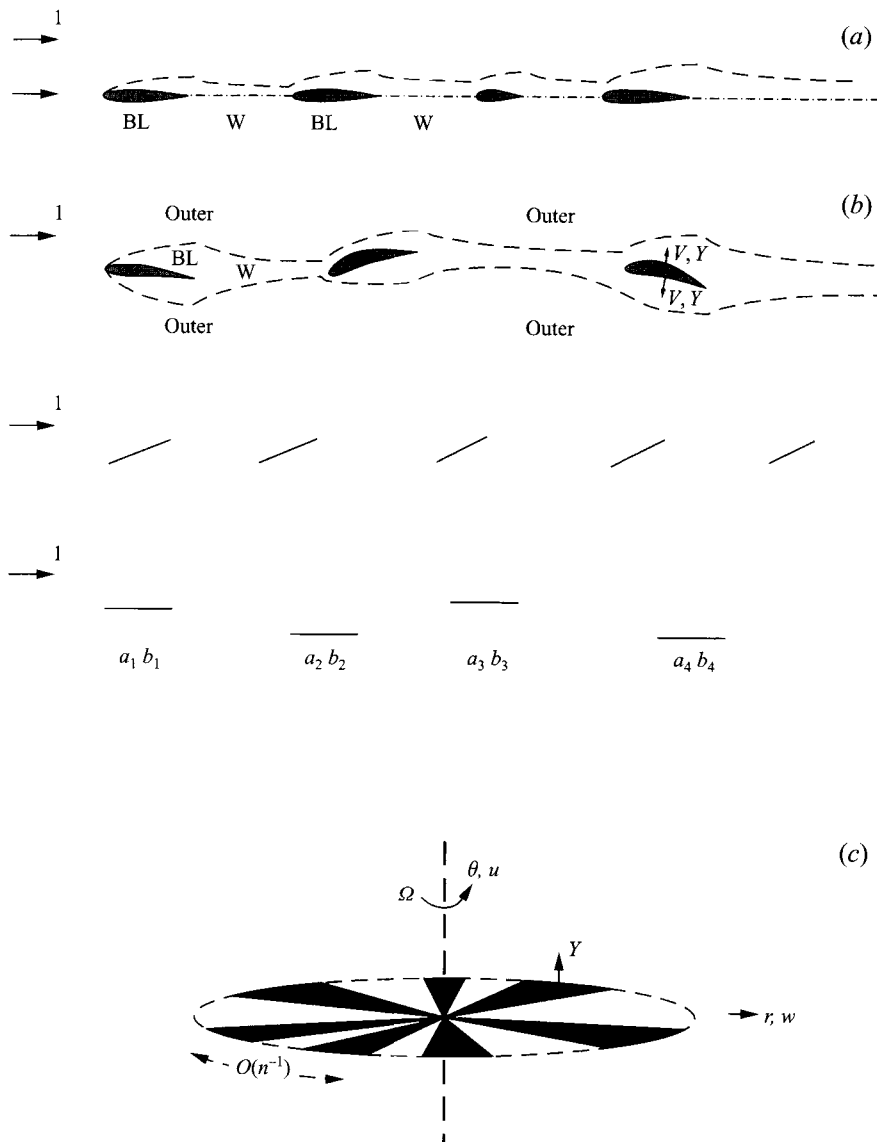


FIGURE 1. Schematic diagrams of the multi-blade flows considered: see §2. (a) Symmetric two-dimensional configurations of thin blades/airfoils with BL, W denoting successive boundary layers and wakes respectively. (b) Examples of non-symmetric two-dimensional configurations, for which the outer potential flow interacts with the BL, W flow. (c) Rotary-blade application in three-dimensional flows, for  $n$  blades; the angular velocity  $\Omega$  is normalized to one.

in turn. There is also a starting condition at the first leading edge,

$$u = 1 \text{ at } x = 0, \text{ for } Y \neq 0. \tag{2.1f}$$

The characteristic boundary-layer coordinate  $Y$  used above in the normal direction is given by  $y = Re^{-1/2}[f(x) + Y]$  on the blades, with  $f$  replaced by zero in the wakes because of symmetry, and the traditional Prandtl shift property is taken. Again, the effective leading-order pressure is zero in each boundary layer and wake partly because the outer flow is disturbed by an amount of only  $O(Re^{-1/2})$  (due to the blade

thicknesses  $f(x)$  added to the unknown viscous displacement thicknesses  $\delta(x)$ , in terms of its velocities and pressures, and partly because  $\partial p/\partial Y$  is negligible in the boundary layers and wakes. In consequence, the thickness dependence  $f(x)$  has no effect at this level, unlike in (§2.2) below. The flow solution outside the BL's and wakes is covered by (§2.2) below.

The problem posed above, namely (2.1a–f), is parabolic in  $x$ , it being assumed that  $u$  is non-negative everywhere. One of the solution properties to be found is the effective viscous displacement  $\delta(x)$ , satisfying

$$\Psi \sim Y - \delta(x), \quad V \rightarrow \delta'(x) \text{ as } Y \rightarrow \infty, \quad (2.2)$$

where the unknown  $\Psi$  is the stream function given by  $u = \partial\Psi/\partial Y$ ,  $V = -\partial\Psi/\partial x$ ,  $\Psi = 0$  at  $Y = 0$ . Another unknown property is the blade-surface shear stress,  $\tau_w \equiv \partial u/\partial Y$  evaluated at  $Y = 0$ , in normalized terms, and likewise for the unknown wake-centrelines velocity  $u_w \equiv u$  at  $Y = 0$ . The task involved above is a numerical one in general, although well-known analytical features hold near each leading and trailing edge, and in far wakes for example, while helpful analytical properties are found later to apply far downstream if  $n$  is large. Solution properties are addressed in §3.

## 2.2. Two-dimensional motions, non-symmetric

A new aspect arises with non-symmetric configurations, such as in figure 1(b). Here the typical angle of incidence of the typical blade, and its typical thickness, camber and displacement, are all taken to be of order  $Re^{-1/2}$ , comparable with the characteristic boundary-layer thickness. Hence the flow in the outer inviscid region ( $x, y \sim 1$ ) consists of an  $O(Re^{-1/2})$  perturbation of the uniform stream,

$$[u, v, p] = [1, 0, 0] + Re^{-1/2}[u_1, v_1, p_1] + \dots, \quad (2.3)$$

leading to Laplace's equation for (say) the pressure

$$(\partial_x^2 + \partial_y^2)p_1 = 0 \quad (2.4a)$$

for  $y > 0$  and  $y < 0$ , at all  $x$ . The boundary conditions on (2.4a) are

$$p_1 \rightarrow 0 \text{ in the far field,} \quad (2.4b)$$

$$p_{1y} = -f''_{\pm}(x) - \delta''_{\pm}(x) \text{ at } y = 0 \pm \text{ on blades,} \quad (2.4c)$$

$$p_1(x, 0+) = p_1(x, 0-) \text{ in wakes.} \quad (2.4d)$$

Here (2.4c) is a matching condition (using  $v_{1x} = -p_{1y}$ ) approximately equivalent to the tangential-flow or efflux constraint as verified below, while (2.4d) is necessary since the pressure jump that each wake can support is typically only  $O(Re^{-1})$  at most. The boundary layer on every blade surface is governed by (2.1a–e) again and likewise for the wakes (with  $(V, Y) \rightarrow (-V, -Y)$  where required), but the wake shapes/centre-lines are now unknown, as is the whole inviscid solution. Above we have supposed each blade to be described by  $y = \pm f_{\pm}(x)$  on its upper and lower surface respectively, with the corresponding displacement thickness  $\pm \delta_{\pm}(x)$  affected by the boundary-layer equations (see (2.2)). The counterparts of  $(f_{\pm} + \delta_{\pm})$  in the wakes, however, along with the jump values  $p_1(x, 0+) - p_1(x, 0-)$  on the blades, are unknown, coupling (2.1a–e) with (2.4a–d) since solving the boundary-layer equations on every succeeding blade requires a starting profile from the previous wake and that depends on the wake centre-line which is one of the unknowns here. Generally, then, neither the viscous

nor the inviscid contribution can be determined without the other, as anticipated in Smith & Timoshin. The new feature therefore is that of inner–outer interaction.

With a single blade the matter simplifies considerably. Because of the Prandtl shift the viscous boundary layer on either surface is of Blasius type then and the viscous wake is of the usual external form, starting from the Goldstein near-wake and extending to the Goldstein far-wake solution far downstream. The actual wake centreline shape  $y = f(x)$ , for  $x > 1$ , is then fixed by the inviscid part (2.4a–d) with  $\delta_{\pm}(x)$  given for all positive  $x$  and zero for all negative  $x$ . See also Brown & Stewartson (1970, 1975), Spence (1970), Messiter & Stewartson (1972). Thus the inner–outer interaction virtually disappears then.

With multiple blades, on the other hand, there is a non-trivial inner–outer interaction. Although the first-blade boundary layers can again be taken to be of the Blasius type in view of the Prandtl shift, and the first-wake solution (ahead of the second plate) similarly is that behind a single plate (albeit with an unknown Prandtl shift), the second-blade boundary layers, wake and so on, all require solution of (2.4a–d) hand-in-hand with (2.1a–e). This is tackled in §4. It covers a wide variety of multiple-blade arrangements such as those indicated in figure 1(b).

### 2.3. Relevance to three-dimensional rotary multi-blade flows

The governing equations for the three-dimensional viscous boundary layers and wakes produced by a rotating system of  $n$  thin blades are verified by Smith & Timoshin (1996) to be the three-dimensional boundary-layer equations supplemented by Coriolis forces, under the assumption of  $O(Re^{-1/2})$  typical blade thicknesses. This is in a rotating frame, with  $Re$  being based on the rotation rate and typical blade chord. The corresponding flow outside the BL's and wakes is governed by a three-dimensional Laplacian problem for the  $O(Re^{-1/2})$  outer pressure disturbance. See figure 1(c). At large non-dimensional radial distances  $r$  however the radial, azimuthal and normal velocities respond as  $r^m$  ( $m = 1, 1, 0$  in turn) times  $w, u, v$  say, yielding the viscous scaled controlling equations as

$$2w + V_Y + u_{\theta} = 0, \quad (2.5a)$$

$$uu_{\theta} + Vu_Y + 2w(u - 1) = u_{YY}, \quad (2.5b)$$

$$uw_{\theta} + Vw_Y + w^2 - (u - 1)^2 = w_{YY}, \quad (2.5c)$$

in the boundary layers and wakes, if the typical blade chord also increases linearly with  $r$  (giving so-called radial blades, whose practical relevance is discussed by Smith & Timoshin 1996 and briefly in the next paragraph). Above,  $\theta$  denotes the angular variable about the axis of rotation, and non-symmetric boundary conditions apply at  $Y = 0, \pm\infty$  in general. Along with this the outer-flow equations become in scaled form

$$(\tilde{y}^2 + 1)\tilde{p}_{\tilde{y}\tilde{y}} - \tilde{y}\tilde{p}_{\tilde{y}} + \tilde{p}_{\theta\theta} + \tilde{p} = 0, \quad (2.6a)$$

subject to matching with the viscous solution and with the far field and to zero pressure jump across the wakes,

$$\tilde{p}_{\tilde{y}} = -\tilde{V}'_{\pm}(\theta) \text{ at } \tilde{y} = 0\pm, \quad (2.6b)$$

$$\tilde{p} \rightarrow 0 \text{ in the far field,} \quad (2.6c)$$

$$\tilde{p} \text{ continuous across } \tilde{y} = 0 \text{ in wakes.} \quad (2.6d)$$

Here  $\tilde{V}$  is analogous with the efflux/thickness effects in (2.4c). The coupled system (2.5a–c), (2.6a–d) holds in the two-dimensional planes  $Y, \theta, \tilde{y}, \theta$ , with periodicity of  $2\pi$  in  $\theta$  also being required.

Concerning the links between this type of three-dimensional rotary motion and the two-dimensional model problems, cases (a) and (b) in §§2.1, 2.2, clearly inner–outer interaction is a common feature and so the ideas used subsequently in §4 in solving for case (b) are expected to apply in the rotary setting, with  $\theta$  replacing  $x$ . In addition there are two contenders/extremes of more direct relevance. One is for comparatively short chords. There all the length scales, for  $Y, \tilde{y}, \theta$ , compress as in Smith & Timoshin’s short-blade limit to leave us with the governing equations of case (b) in general or (a) if there is normal symmetry. The requirement of  $2\pi$ -periodicity in  $\theta$  still stands however and that generally restricts the relevance of (a), (b) here to a finite group or groups of rotating short-chord blades occupying a small fraction of the  $2\pi$  range in  $\theta$ , apart from the case of an isolated blade or blades where interaction becomes suppressed (see §2.2). The other extreme is the many-blade limit in Smith & Timoshin, for which  $n$  is large. There the boundary layer itself becomes double-structured, with a displaced form of the von Kármán  $\theta$ -independent solution holding in the bulk of the boundary layer whereas in an inner tier the response is fast-varying including dependence on  $\tilde{\theta}$  where  $\tilde{\theta} = n\theta$ . This means, in terms of the unknown functions in (2.6a–d),

$$\tilde{V}_{\pm} \sim -n^{2/3} b'_{\pm}(\tilde{\theta}), \quad \tilde{p} \sim n^{2/3} p_*, \quad \tilde{y} = n^{-1} y_*, \quad (2.7a)$$

for large  $n$ . Substitution into (2.6a–d) then confirms that the controlling equations (2.4a–d) given earlier in §2.2 apply now to  $p_*(\tilde{\theta}, y_*)$ . Moreover the effective upper and lower displacements  $-b_{\pm}(\tilde{\theta})$  depend again on the viscous-layer properties similarly to those described in §2.2. The only differences are that here, in effect,

$$u \sim \pm(Y - f_{\pm}(\tilde{\theta}) + b_{\pm}(\tilde{\theta})) \text{ as } Y \rightarrow \pm\infty \quad (2.7b)$$

because of the sublayer behaviour, cf. (2.1e), (2.2), and the starting profile is unknown in advance, cf. (2.1f). The connection between the uniform-shear condition (2.7b) and the uniform-stream conditions in §§2.1, 2.2 is actually cemented in §§3,4. We observe also the links between the two extremes just considered.

Our task, then, is to solve the viscous system (2.1a–f) but coupled with the inviscid system (2.4a–d) in non-symmetric cases as studied in the next two sections.

### 3. Symmetric-flow properties

With a symmetrical arrangement of blades and with a symmetric-flow solution assumed §2.1 holds, implying that (2.1a–f) are to be solved. To the present order, and taking account of comments in §§2.1,2.2 on the Prandtl shift, the Blasius form can be presumed to apply over the entire first blade (blade 1) followed next by a standard single-blade wake (wake 1) but the latter persists only to the leading edge of the second blade. Thereafter computational solutions are necessary, over blade 2, wake 2, blade 3, wake 3, and so on; note that here the distortion of the blade-1 flow solution from the outer flow of (2.4a–d) is a higher-order effect.

For the computations we took a semi-explicit finite-difference approach of nominal second-order accuracy as in Smith & Timoshin (1996). The reason for this choice is, as in that paper, the combination of robustness and accuracy produced, including the ability to handle well all the leading and trailing edges present in the multi-blade motion. The chief part of the treatment revolves around discretizing the momentum

equation (2.1b) as

$$\bar{u}_j(u_j - \bar{u}_j)/\Delta + \bar{V}_j(u_{j+1} - u_{j-1})/2h = (u_{j+1} - 2u_j + u_{j-1})/h^2 \quad (3.1a)$$

where  $u_j$  ( $j = 1$  to  $J$ ) are the unknown  $u$  quantities at the current  $x$ -station, for  $Y$  values  $(j - 1)h$  with step size  $h$ , and the overbar denotes quantities known at the previous station  $(x - \Delta)$ . Along with two boundary conditions from (2.1c or d,e), (3.1a) serves to fix all the  $u_j$  after which a discretization of the continuity equation (2.1a) with (2.1c or d) determines the new  $V_j$ 's at  $x$ . The above is second-order accurate in  $Y$  but only first order in  $x$  as it stands. Second-order  $x$ -accuracy is obtained however by a simple double-step procedure, with two steps of length  $\Delta/2$  from  $(x - \Delta)$ , followed by extrapolation in  $\Delta$ . Schematically, if (3.1a) gives predictor values  $u^{(p)}(\Delta)$ , say, then the corrector (c) double-step takes

$$\bar{u} \rightarrow u^{(p)}\left(\frac{1}{2}\Delta\right) \rightarrow \frac{1}{2}\{u^{(c)}(\Delta) + u^{(p)}(\Delta)\}, \quad (3.1b)$$

yielding  $u^{(c)}(\Delta)$  of order  $\Delta^2$  accuracy;  $V$  is treated similarly. Throughout, the forward-differencing of the viscous term as in (3.1a) seems to render the treatment notably stable compared with other methods, as well as accurate.

The starting condition (2.1f) is imposed directly in the form  $\bar{u}_j = 1$ , with  $\bar{V}_j = 0$ ,  $j \geq 2$  at the start of the run. The Blasius-like response then emerges accurately in two steps or so downstream effectively. Similarly at all the subsequent leading and trailing edges no special treatment is required, as the computations proceed by forward-marching in  $x$ . Tests showed that, by and large, a step size of about 0.005 in  $x$  with a  $Y$ -grid of about  $401 \times 0.05$  is adequate for most purposes except possibly far downstream when many blades are present.

Computational results are presented in figures 2 and 3. Here, to repeat, we may take the blade thickness(es)  $f(x)$  to be zero without loss of generality in this current symmetric setting. That nevertheless leaves an enormous variety of configurations which could be examined, of course, depending on the number ( $n$ ) of blades, their individual chord lengths ( $\ell_c$ ) and their individual gaps or wake lengths ( $\ell_w$ ). In the present study,  $n, \ell_c, \ell_w$  are varied only so far as to show the dominant flow features of concern: again see figures 2 and 3, where blade  $n$  occupies the interval  $(a_n, b_n)$  of the  $x$ -axis,

$$0 = a_1 < b_1 < a_2 < b_2 < a_3 < b_3 < \dots, \quad (3.2)$$

so that each  $\{\ell_c, \ell_w\}$  pair equals  $\{(b_n - a_n), (a_{n+1} - b_n)\}$ .

Analytically there are at least seven main extremes (i)–(vii) of interest, as follows. First, (i) is the flow response just downstream of each leading edge. The response is clearly of the Blasius form locally but with the free-stream input value, i.e. 1 in (2.1f) for blade 1, replaced by (reduced to) the centreline wake velocity  $u(a_n-, 0)$  for blade  $n$ , when  $(x - a_n)$  is small and positive. Higher-order terms are provoked by the non-zero curvature of the input velocity profile, cf. section 4. The response seems evident in the results in fig.2, including the gradual increase in the typical  $\delta$  and  $V_\infty$  locally due to the gradual (continual) decrease in input velocity. Next, (ii) concerns the behaviour just beyond each trailing edge. Again the response is locally as for a single airfoil but subject to a renormalization, this time associated with the altered surface shear stress just ahead of each trailing edge, exactly as in Goldstein's (1930) near-wake analysis. The behaviour again seems evident in the computed results. The third extreme (iii) is for a relatively large gap or gaps,  $\ell_w \gg 1$ . In this case the corresponding wake solution approaches closely the uniform-stream state  $u \equiv 1$  for all  $Y$  (Goldstein's far wake), downstream, and so the flow on the next blade commences anew exactly as for blade

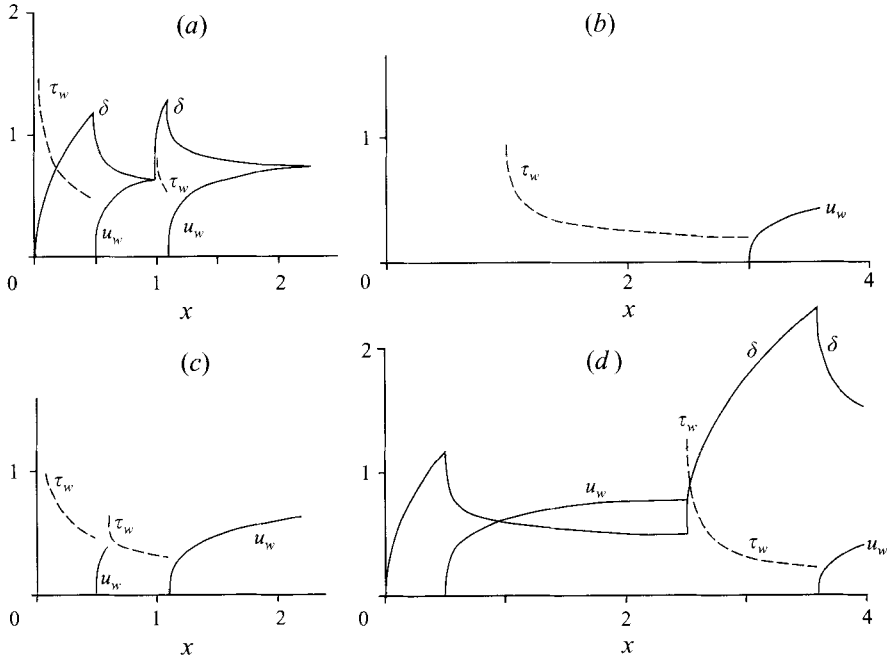


FIGURE 2. Solutions computed for four symmetric arrangements, with two blades 1,2, showing  $\tau_w, u_w, \delta$  versus  $x$ . The values of  $[a_1, b_1, a_2, b_2]$  are (a)  $[0, 0.5, 1, 1.1]$  (relatively short blade 2), (b)  $[0, 0.5, 1, 3]$  (relatively long blade 2). (c)  $[0, 0.5, 0.6, 1.1]$  (relatively short wake 1), (d)  $[0, 0.5, 2.5, 3.58]$  (relatively long wake 1). The solutions on blade 1 are the same in all cases.

1, to leading order, in view of (2.1f). The fourth extreme (iv) is for a relatively small gap,  $\ell_w \ll 1$ . As in Smith & Timoshin however this has little effect except quite close to the succeeding leading edge, as figure 2 demonstrates. Fifth, (v) concerns small chords,  $\ell_c \ll 1$ , but likewise the effect is only local. Sixth, (vi), if the chord is large so that  $\ell_c \gg 1$  then generally the flow solution on the blade nears the thickening Blasius form downstream. The subsequent wake therefore starts as does wake 1, to leading order. Subsequent blades however may then act as if short-chord ones in effect. Most of the above extremes are reflected in figure 2. The seventh and final extreme, (vii), is associated with many blades, where  $n \gg 1$ , cf. figure 3, and that is the extreme of most interest which is examined in the rest of this section.

When  $n$  is large, a double scaling in  $x$  and a two-tiered structure in  $Y$  emerge downstream. Near the  $m$ th blade, say, with  $m$  large, the two streamwise scales represent relatively slow dependence on  $x_1$ , where  $x = mx_1$ , accompanied by relatively fast dependence on the local  $x = X$  around the blade. Hence

$$\partial_x \rightarrow \partial_X + m^{-1} \partial_{x_1} + \dots \quad (3.3)$$

It is assumed that the typical blade chords here remain  $O(1)$  throughout. At these streamwise distances of order  $m$  downstream a normal viscous scale of order  $m^{1/2}$  is to be expected, then, but viscous sublayers are also present because of the continual leading-edge and trailing-edge adjustments taking place over streamwise distances of order one. So two tiers I and II emerge in the  $Y$ -direction, as in figure 4(a). The outer tier I has normal scale  $O(m^{1/2})$  as expected, whereas that of the inner tier II is  $O(m^{1/6})$ . The latter scale emerges because of the viscous-inviscid balance of operators

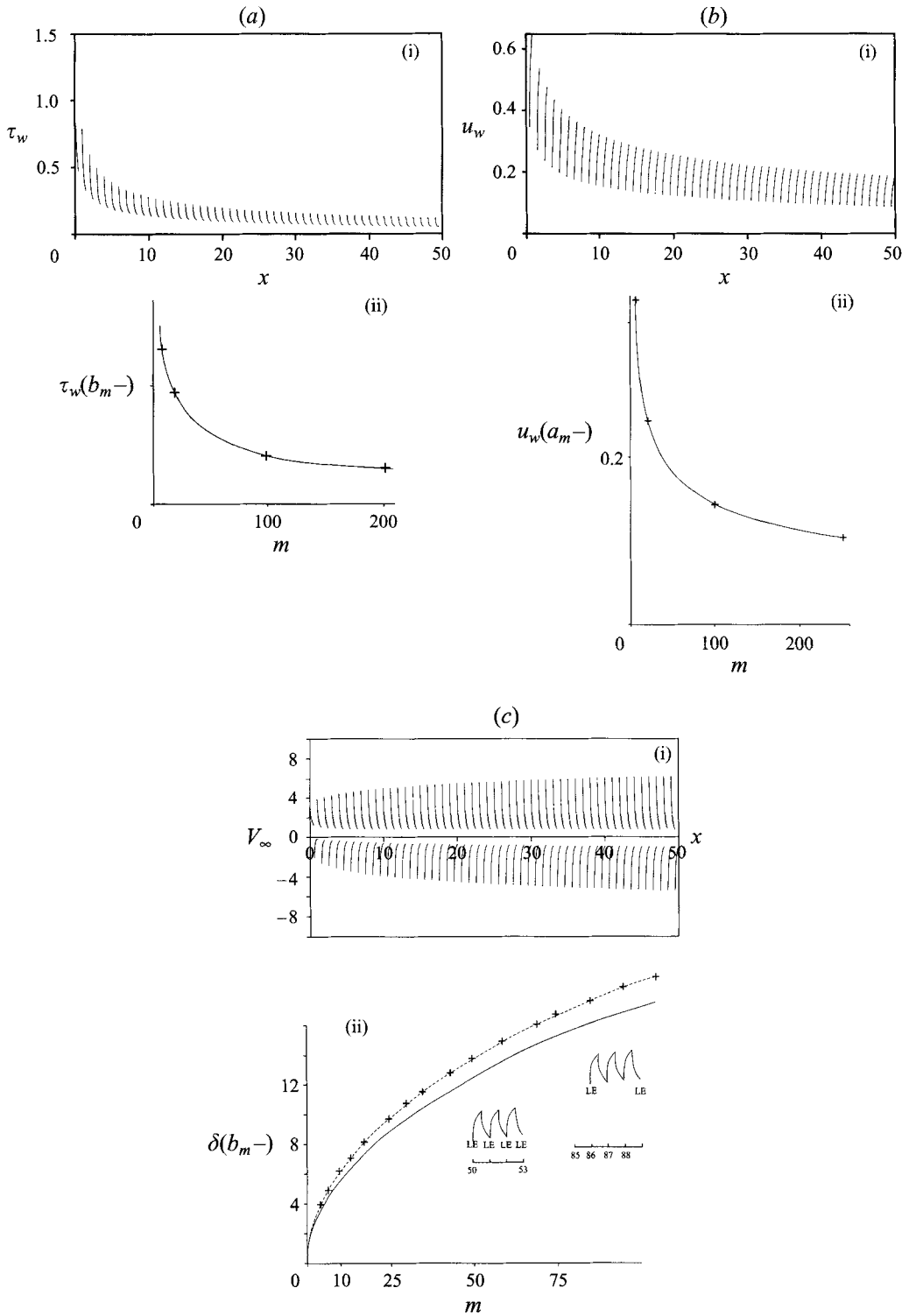


FIGURE 3. For caption see facing page.

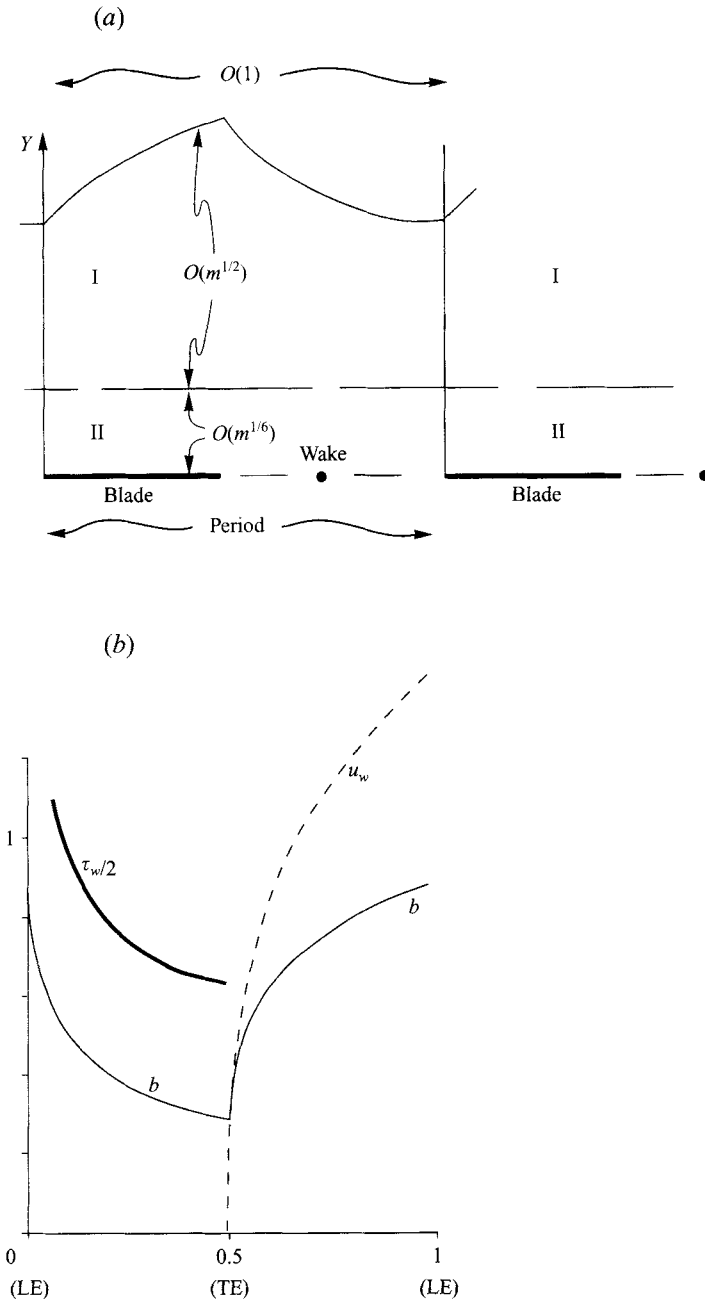


FIGURE 4. (a) Flow structure for large  $m$ , including tiers I and II. (b) Normalized solution of the limit problem (3.8a-f) appropriate to the case of figure 3.

FIGURE 3. Computational results and comparisons for a symmetric arrangement of many blades, with  $[a_m, b_m] = [m-1, m-\frac{1}{2}]$  for  $m \geq 1$ , so that  $\ell_c = \ell_w = \frac{1}{2}$ . (a) (i),  $\tau_w$  against  $x$  on blades 1-50; (ii),  $\tau_w$  at  $x = b_m$ —(solid curve) compared with large- $n$  theory (shown +, obtained from figure 4 below). (b) (i),  $u_w$  against  $x$  in wakes 1-50; (ii),  $u_w$  at  $a_m$ —(solid) compared with large- $n$  theory (+, from figure 4). (c) (i), efflux  $V_\infty$  against  $x$  for blades and wakes 1-50; (ii),  $\delta$  at  $b_m$ —(solid) compared with large- $n$  leading/mean term (+ — —, from figure 4). The insets show close-ups of  $\delta$  near  $x = 50, 85$ , using the same vertical scale.

$u\partial/\partial x \sim \partial^2/\partial Y^2$  combined with  $x$  being  $O(1)$  and  $u$  being  $O(Y/m^{1/2})$  from the outer tier, implying the balance  $Ym^{-1/2} \sim Y^{-2}$  and hence  $Y \sim m^{1/6}$ , while  $u$  is therefore of order  $m^{1/3}$  in the inner tier and  $V$  follows from the continuity balance.

In tier I covering the majority of the blade-wake flow  $Y = m^{1/2}\tilde{Y}$  and

$$u = U_0(x_1, \tilde{Y}) + m^{-1/3}U_e(X, \tilde{Y}) + \dots + m^{-1}U_1(X, \tilde{Y}) + \dots, \quad (3.4a)$$

$$V = m^{1/6}V_e(X, \tilde{Y}) + \dots + m^{-1/2}V_1(X, \tilde{Y}) + \dots. \quad (3.4b)$$

Here all the components are unknown,  $U_0$  being independent of the fast scale  $X$ . From substitution into (2.1a,b) however

$$U_e = b(X)\partial U_0/\partial \tilde{Y}, \quad V_e = -(db/dX)U_0, \quad (3.4c)$$

corresponding to a small displacement effect or Prandtl shift with  $U_0$  evaluated at  $\tilde{Y} + m^{-1/3}b(X) + \dots$  in place of  $\tilde{Y}$  in (3.4a), where the unknown function  $b(X)$  depends on the fast streamwise variable. Similar considerations apply to other such extra terms in (3.4a,b), until the continuity and momentum balances

$$\partial U_1/\partial X + \partial U_0/\partial x_1 + \partial V_1/\partial \tilde{Y} = 0, \quad (3.5a)$$

$$U_0(\partial U_1/\partial X + \partial U_0/\partial x_1) + V_1\partial U_0/\partial \tilde{Y} = \partial^2 U_0/\partial \tilde{Y}^2, \quad (3.5b)$$

effectively, are reached at higher order. These balances contain both short- and long-scale variations. We suppose now that there is a short-term periodicity in the motion, over a range  $L$  in  $X$ , for instance if all the blades have equal chord as in some of the computations described earlier or if their configuration repeats itself after a distance  $L$ , far downstream. Then integration with respect to  $X$  over the period yields, from (3.5a,b),

$$\partial U_0/\partial x_1 + \partial \langle V_1 \rangle / \partial \tilde{Y} = 0, \quad (3.6a)$$

$$U_0\partial U_0/\partial x_1 + \langle V_1 \rangle \partial U_0/\partial \tilde{Y} = \partial^2 U_0/\partial \tilde{Y}^2 \quad (3.6b)$$

in which the angled brackets denote the mean value over the period. The governing equations (3.6a,b) together with the boundary conditions

$$U_0 = \langle V_1 \rangle = 0 \text{ at } \tilde{Y} = 0+, \quad U_0 \rightarrow 1 \text{ as } \tilde{Y} \rightarrow \infty, \quad (3.6c)$$

form the main long-scale nonlinear problem at this stage. The relevant solution is the Blasius one

$$U_0 = f'(\eta), \quad \langle V_1 \rangle = \frac{1}{2}(\eta f' - f)x_1^{-1/2}, \quad \eta \equiv \tilde{Y}x_1^{-1/2}, \quad (3.6d)$$

where  $f$  is the Blasius function. The argument here and below is an extension of that in Smith & Timoshin (1996) (cf. Riley 1996), including the reasoning behind the constraints at  $\tilde{Y} = 0+$  in (3.6c).

In tier II, the sublayer near the typical blade and wake,  $Y = m^{1/6}Y_*$  and the behaviour of (3.4a-c) with (3.6a-d) at small  $\tilde{Y}$  implies the expansions

$$u = m^{-1/3}U_* + \dots, \quad V = m^{-1/6}V_* + \dots. \quad (3.7)$$

Substitution into (2.1a,b) now gives the main short-scale nonlinear problem as

$$\partial U_*/\partial X + \partial V_*/\partial Y_* = 0, \quad (3.8a)$$

$$U_*\partial U_*/\partial X + V_*\partial U_*/\partial Y_* = \partial^2 U_*/\partial Y_*^2, \quad (3.8b)$$

subject to the conditions

$$U_* = V_* = 0 \text{ at } Y_* = 0 \text{ on blades}, \quad (3.8c)$$

$$\partial U_*/\partial Y_* = V_* = 0 \text{ at } Y_* = 0 \text{ in wakes,} \quad (3.8d)$$

$$\partial U_*/\partial Y_* \rightarrow \lambda \text{ as } Y_* \rightarrow \infty, \quad (3.8e)$$

$$L\text{-periodicity in } X. \quad (3.8f)$$

Here (3.8c,d) follow from (2.1c,d), which (3.8e) is to match with the majority solution in tier I and (3.8f) is required as stated previously. The  $O(1)$  shear factor  $\lambda$  equals  $\partial u_0/\partial \tilde{Y}$  evaluated at  $\tilde{Y} = 0+$  and so is quasi-constant within this short-scale problem; specifically  $\lambda = f''(0)x_1^{-1/2}$  from (3.6d). The solution of (3.8a–f) is given numerically by Smith & Timoshin for a representative local configuration. A computational solution for a configuration of current interest is presented in our figure 4(b) (with  $\lambda$  normalized to unity). As part of the solution the negative displacement effect  $b(X)$  is determined, in the form

$$U_* \sim \lambda(Y_* + b), \quad V_* \sim -\lambda Y_* db/dX \text{ as } Y_* \rightarrow \infty, \quad (3.9)$$

in line with the contributions in (3.4a–c). We observe also the mean-shear result

$$\langle \tau_w \rangle = \lambda \quad (3.10)$$

on each blade, as in the last paper. Comparisons between the present large- $n$  analysis and the earlier computations may be made in terms of the  $\tau_w, u_w, \delta$  distributions for example and the agreement found is fairly supportive even at moderate  $n$  values of 5 or less, as indicated earlier in figure 3.

It is noteworthy first here that both of the tiers I, II above are viscous ones, as described in (3.6a,b), (3.8a,b) respectively, and second that the Blasius solution still emerges in the mean downstream, within the outer tier I. Given all the gaps present between the blades, the second feature above may seem suprising initially, but in a sense the inner viscous tiers II continually protect the thicker outer viscous tiers I from the full impact of each leading and trailing edge, except for the fast-varying displacement (with zero mean) induced locally. Further on that theme, Blasius flow can even be produced if the total amount of blade surface(s) is asymptotically small compared with the total amount of gap(s). Third, we note the connection in tier II with the boundary condition (2.7b) in §2.3. Finally, the large- $n$  approach also proves useful in §4 below, while issues of drag and sheltering effects are covered in §§5 and 6.

#### 4. Non-symmetric-flow properties

In the non-symmetric case as described in §2.2 inner–outer interaction occurs, requiring the viscous inner part (2.1a–f) to be coupled with the inviscid outer part (2.4a–d). Since the latter part is linear it is sufficient to deal with the non-symmetric contribution there.

Thus, with  $\hat{P} \equiv p_1^{(+)} - p_1^{(-)}$  where  $+, -$  refer to the half-planes  $y > 0, y < 0$  respectively,  $\hat{P}(x, y)$  satisfies Laplace's equation in the upper half-plane but subject to

$$\hat{P}(x, 0) = 0 \text{ in intervals } (-\infty, 0), (b_1, a_2), (b_2, a_3), \dots, \quad (4.1a)$$

$$\frac{\partial \hat{P}}{\partial y}(x, 0) = -\hat{V}'(x) \text{ in intervals } (a_1, b_1), (a_2, b_2), \dots. \quad (4.1b)$$

Here (4.1a,b) correspond to the wake and blade conditions (2.4c,d) in turn, and the

unknown function

$$\hat{V}(x) \equiv (f + \delta)'_+ - (f + \delta)'_- = \left\{ v_1^{(+)} - v_1^{(-)} \right\} (x, 0) \tag{4.2}$$

which is equivalent to the difference in normal velocities at the upper and lower edges of the boundary layers or wakes in view of the viscous part, cf. (2.2), (2.6*b*). Only the unknown difference function in (4.2) influences the flow response, rather than the individual  $f$  and  $\delta$ . In addition to (4.1*a,b*) an analogue of (2.4*b*) holds also. The chief inviscid result now follows, for example from treating  $\hat{P} + i \left\{ v_1^{(+)} - v_1^{(-)} \right\}$  as a complex function  $\mathcal{F}(z)$  of  $z = x + iy$  in  $y > 0$ , given the Cauchy–Riemann equations satisfied by its real and imaginary parts, and then considering multiplying or dividing  $\mathcal{F}$  by  $\frac{1}{2}$  powers of  $(z - a_n)$ ,  $(z - b_n)$ ; see also Muskhelishvili (1946). A Kutta condition is applied at each trailing edge. We thereby obtain the relations

$$\left. \begin{array}{l} -\pi \hat{P}(x, 0) \\ \text{or} \\ \pi \left\{ v_1^{(+)} - v_1^{(-)} \right\} (x, 0) \end{array} \right\} = \left| \frac{(x - b_1)(x - b_2) \dots (x - b_n)}{(x - a_1)(x - a_2) \dots (x - a_n)} \right|^{1/2} \sum_{N=1}^n \int_{a_N}^{b_N} \frac{\hat{V}(\xi)}{(x - \xi)} \left| \frac{(\xi - a_1) \dots (\xi - a_n)}{(\xi - b_1) \dots (\xi - b_n)} \right|^{1/2} d\xi \tag{4.3a, b}$$

first for the induced pressure jumps on the  $n$  blades  $(a_1, b_1), (a_2, b_2), \dots$ , in (4.3*a*), and second for the velocity jumps across the gaps (wakes) in  $(-\infty, 0), (b_1, a_2), (b_2, a_3), \dots$  in (4.3*b*).

As far as solving the interaction equations is concerned, (4.3*b*) is the more relevant. It is to be combined with the boundary-layer equations (2.1*a-f*) on each blade surface and wake in an iterative scheme to determine  $\delta_+ - \delta_-$  for all  $x$  and  $f_+ - f_-$  in the wakes (fixing the unknown wake centreline shapes), among other quantities, given  $f_{\pm}$  on all the blades. The other relation, (4.3*a*), is used afterwards to find the induced pressure differences and hence the lift, as in §5 later.

Before describing computational solutions it is worth considering the local behaviour near each leading and trailing edge, where  $x \sim a_n, b_n$ . Based on the inviscid properties just above which stem from (2.4*a-d*) the expected responses are of the form

$$\hat{P}(x, 0) = 0, \quad O(x - a_n)^{-1/2}, \quad O(b_n - x)^{1/2}, \quad 0, \tag{4.4a}$$

$$\hat{V}(x) - \text{constant} = O(a_n - x)^{-1/2}, \quad o(x - a_n)^{-1/2}, \quad o(b_n - x)^{1/2}, \quad O(x - b_n)^{1/2}, \tag{4.4b}$$

as  $x \rightarrow a_n^-, a_n^+, b_n^-, b_n^+$  in turn. Concerning the corresponding viscous properties, with which (4.4*a,b*) must comply, we examine the leading-edge behaviour of the characteristic blade- $n$  boundary layers on the upper and lower surfaces, assuming the latter to be relatively flat for the sake of argument but the incident wake flow to be non-symmetric. So the starting profile for the  $n$ th boundary layers of (2.1*a-e*) is  $u = u_0(Y)$ , say, with  $u_0(\pm\infty) = 1$  and

$$u_0(Y) \sim c_0 + c_1 Y + c_2 Y^2 + \dots \text{ for } Y \ll 1, \tag{4.5}$$

where the coefficients are non-zero in general. The response at small positive  $(x - a_n)$  on the upper surface is then two-zoned. An outer zone has  $Y$  of order unity and

$$\Psi = \Psi_0(Y) + (x - a_n)^{1/2} \Psi_1(Y) + (x - a_n) \Psi_2(Y) + \dots, \tag{4.6a}$$

with  $u_0 = \Psi'_0$  and  $\Psi_0(0) \equiv \kappa$  (say) being non-zero in most cases. Substitution into

(2.1a,b) yields the solutions

$$\Psi_1 = \Gamma_1 u_0, \quad (4.6b)$$

$$\Psi_2 = \Gamma_2 u_0 + u_0 \int_0^Y u_0'' u_0^{-2} dY + \frac{1}{2} \Gamma_1^2 u_0', \quad (4.6c)$$

where  $\Gamma_1, \Gamma_2$  are constants to be determined. Hence at small  $Y$  the limits  $\Psi_1 \rightarrow \Gamma_1 c_0$ ,  $\Psi_2 \rightarrow \Gamma_2 c_0 + \Gamma_1^2 c_1/2$  hold. This outer zone is mainly inviscid. The inner viscous zone then has  $Y = (x - a_n)^{1/2} \bar{\eta}$  with  $\bar{\eta}$  of  $O(1)$  and

$$\Psi = \kappa + (x - a_n)^{1/2} f_0(\bar{\eta}) + (x - a_n) f_1(\bar{\eta}) + \dots \quad (4.7a)$$

Here, again from (2.1a-e),  $f_0$  is the Blasius function  $f$  as in (3.6d) but satisfying  $f_0'(\infty) = c_0$ , while  $f_1$  satisfies

$$f_1''' + \frac{1}{2} f_0 f_1'' - \frac{1}{2} f_0' f_1' + f_0'' f_1 = 0, \quad (4.7b)$$

subject to  $f_1(0) = f_1'(0) = 0$ ,  $f_1'(\infty) = c_1$ . Solution properties at large  $\bar{\eta}$  are of most concern here, giving

$$f_0 \sim c_0 \bar{\eta} + \beta_0 + \gamma_0(\exp), \quad (4.7c)$$

$$f_1 \sim c_1 \left( \frac{1}{2} \bar{\eta}^2 + \beta_0 c_0^{-1} \bar{\eta} \right) + \beta_1 + \gamma_1(\exp). \quad (4.7d)$$

In (4.7c,d) the leading coefficients  $c_0, c_1$  can be fixed by direct matching with (4.5a), leaving the constants  $\beta_0, \gamma_0, \beta_1, \gamma_1$  then known, while matching with the outer-zone solution yields the results

$$\Gamma_1 = c_0^{-1} \beta_0, \quad \Gamma_2 c_0 + \frac{1}{2} \Gamma_1^2 c_1 = \beta_1 \quad (4.8)$$

for the coefficients  $\Gamma_1, \Gamma_2$ . On the lower surface there is a similar response of course, this being covered by changing the signs of  $\Psi, V, Y$  effectively. In consequence the corresponding coefficients can be evaluated as in (4.6a)–(4.8). Hence, from examination of the differences in  $\Psi$  in the outer zones on the two surfaces, the local value of the difference in viscous efflux velocities at small positive  $(x - a_n)$  is given by

$$V_\infty^{(+)} - V_\infty^{(-)} = (\text{zero})^*(x - a_n)^{-1/2} - \left\{ 2\Gamma_2 + \int_0^\infty u_0'' u_0^{-2} dY - \int_{-\infty}^0 u_0'' u_0^{-2} dY \right\} + \dots \quad (4.9)$$

We observe in particular the zero coefficient of the  $-\frac{1}{2}$  power, which occurs because the  $-\frac{1}{2}$  powered terms in each of  $V_\infty^{(+)}, V_\infty^{(-)}$  cancel and which provides agreement between the viscous and inviscid properties, cf. (4.4b). Further, the influence of the non-symmetric starting profile  $u_0$  is clear in the integral contributions to (4.9). Similar reasoning applies near the  $n$ th trailing edge, as  $x \rightarrow b_n \pm$ , consistent again with (4.4b). The shorter-scale structures holding closer to each leading and trailing edge are mentioned in the next section. We turn now to the computational task.

The variety of flow problems possible is multiply infinite due to all the possible blade shapes and arrangements. We tackle a limited number of course, starting with only two blades. For two blades (1,2), the upper and lower boundary layers on blade 1 are known to be of the Blasius form exactly, possibly Prandtl-shifted, while wake 1 is equivalent to a usual single-blade wake (see §2.2) for the range  $b_1 < x < a_2$  but with

its unknown centreline curve built into the Prandtl shift. Our task is essentially to determine that centreline curve. The task can actually be reduced further, to finding the centreline curve value at  $x = a_2-$  alone. The computational sweeping method, developed from that of §3, proceeds as follows.

(i) March the blade 1 and then wake 1 solutions along to  $x = a_2-$ . Guess the wake centreline shift ( $Y_+ - |Y_-|$ ) at  $x = a_2-$ .

(ii) Integrate the upper- and lower-surface boundary layers along blade 2, from  $a_2+$  to  $b_2-$ , to obtain  $\delta_{\pm}$  distributions along blade 2.

(iii) Compute a new  $\hat{V}(x)$  along blade 2, using (4.2).

(iv) Re-calculate the wake centreline shift at  $x = a_2-$  from an integral of (4.3b) with respect to  $x$ , namely

$$\pi \{Y_+ - |Y_-|\} = \pi f_+(b_1) + \int_{b_1}^{a_2} (\text{RHS}) dx, \quad (4.10)$$

where RHS denotes the right-hand side of (4.3b), with  $n = 2$  in the present case. We recall that  $f_+, f_-$  are equal and opposite for  $b_1 \leq x < a_2$ ,  $b_2 < x$  in this two-blade context, and  $f_+(b_1)$  is given.

(v) Check on convergence; return to (ii) and re-sweep, or finish.

At the start of each sweep in step (ii) accurate interpolation is necessary of the wake profile from (i), in order to split it precisely into the two starting profiles for blade-2's upper and lower surfaces. Apart from that the scheme of §3 then handles each boundary layer on blade 2 satisfactorily, including the leading-edge behaviour. The values of  $\delta_{\pm}$  and  $V_{\infty}^{(\pm)}$  are stored at the successive  $x$ -stations. Step (iii) is straightforward; here in practice we took the edge values  $V_{\infty}^{(\pm)}$  of  $V$  to avoid a differentiation. In step (iv) the integral is evaluated after the substitution

$$x = b_1 \cos^2 \hat{\theta} + a_2 \sin^2 \hat{\theta} \quad (4.11)$$

is made,  $\hat{\theta}$  running from zero to  $\pi/2$ , to cater for the end-point behaviour. In step (v) the convergence criterion used mostly seeks differences of less than  $10^{-7}$  between all the successive  $\delta_{\pm}$  iterates, at given  $x$ .

Results are shown in figure 5, for a number of non-symmetric two-blade configurations. No evidence of non-uniqueness is found, incidentally; on the contrary uniqueness seems indicated by the behaviour during the iterative scheme. For given blade shapes the task above could be simplified (inverted) by specifying the wake centreline shift at  $a_2-$  and then finding that angle of incidence of blade 2 which satisfies (4.10), a simplification which is followed through in the next paragraph. The results shown exhibit up-down symmetry, with respect to changing the sign of both  $f_+(b_1)$ ,  $\alpha$ . They reduce to the results of §3 in symmetric cases. At the other extreme, of relatively high non-symmetry, the results also seem sensible. For example, at large  $\alpha$  the viscous influences from the  $\delta_{\pm}$  thicknesses are expected to become negligible, implying dominance by the inviscid outer properties. A limit calculation for zero  $\delta_{\pm}$  values confirms this. Also from the results the pressure differences can be found from (4.3a), contributing to the lift and drag discussed in the next section.

A related approach was adopted for three blades (1,2,3), placed in several different configurations. The direct task is more difficult then, the effective size of the problem being squared at least since two unknown wake centreline curves must be found. We could have used the procedure (i)–(v) again as the basis, but augmented by the need to integrate further in  $x$ , covering the unknown wake 2 and then blade 3 in order to find the  $V_{\infty}^{(\pm)}$  variations there. That in itself involves a sub-problem of the type (i)–(v)

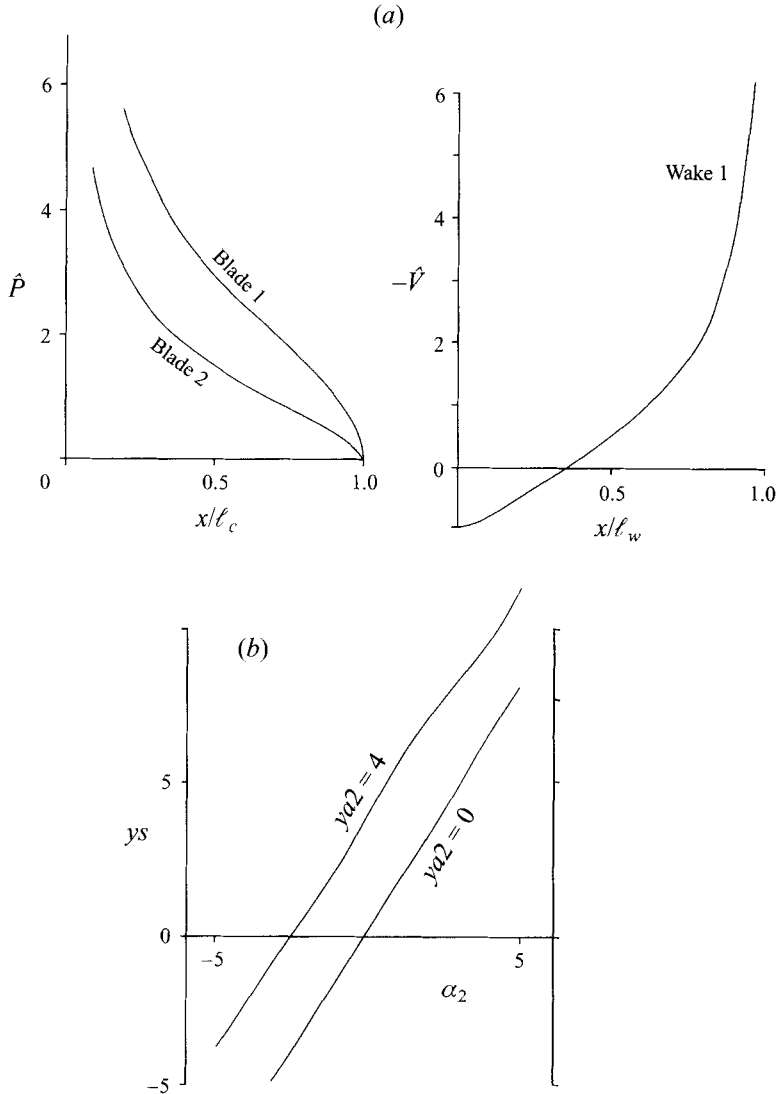


FIGURE 5. Results computed for non-symmetric configurations of two thin blades at incidence. These cases have  $[a_1, b_1, a_2, b_2] = [0, \frac{1}{2}, \frac{3}{2}, 3]$ . (a) Pressure difference  $\hat{P}$  and efflux  $\hat{V}$  along blades 1, 2 and wake 1 respectively, for incidence angles  $\alpha_1 = 1$ ,  $\alpha_2 = 1$  and leading-edge positions  $f(a_1+) = f(a_2+) = 0$ . Note the physically sensible upwash followed by downwash, shown in  $\hat{V}$  and consistent with (4.4a)ff.; also sign reversals of both  $\alpha_1, \alpha_2$  produce sign reversals in  $\hat{P}, \hat{V}$ . (b) Dependence on  $\alpha_2$  of  $y_s$ , the  $Y$ -shift at  $a_2-$ , subtracted from  $f(a_2+)$ , for positions  $f(a_2+)(= \gamma a_2) = 0, 4$ , with zero  $\alpha_1$ .

again. Instead of taking that direct approach we adopted an inverse one hinted at in the previous paragraph. Here the wake centreline  $Y$ -shifts at  $a_2-$ ,  $a_3-$  are specified and the aim then is to find, for given shapes of blade 2 and blade 3, the respective angles of incidence  $\alpha_2, \alpha_3$  corresponding to those two  $Y$ -shifts. In this way only one sweep of the entire nonlinear boundary-layer solution is required, over blade 1 and its wake as before followed by the upper and lower surfaces of blade 2, its wake, and likewise over blade 3. The linearity of the interaction law (4.3b) or (4.10) then enables

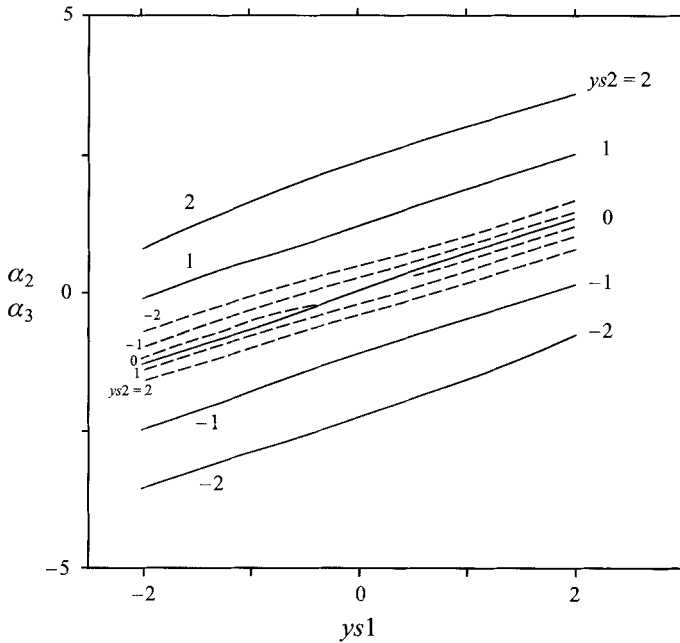


FIGURE 6. Results for non-symmetric configurations of three thin blades at incidence, showing the dependence of  $\alpha_2$  (---),  $\alpha_3$  (—) on the  $Y$ -shifts  $Y_2, Y_3$  at  $a_2-, a_3-$ . Here  $ys1 \equiv f(a_2+) - Y(a_2-)$ ,  $ys2 \equiv f(a_3+) - Y(a_3-)$  and  $\alpha_1$  is zero, while  $[a_1, b_1, a_2, b_2, a_3, b_3] = [0, 1, 3/2, 3, 7/2, 4]$ . See also other properties in figure 7.

the correct  $\alpha_2, \alpha_3$  values to be found readily, in effect adding contributions

$$2\alpha_2 \text{ in } (a_2, b_2), \quad 2\alpha_3 \text{ in } (a_3, b_3), \tag{4.12}$$

to  $V$  in (4.3b), with  $n$  equal to 3 now. The method represents a hinge process of course, swinging blade 2 and blade 3, with their leading edges fixed say, to produce the desired/designed flow properties. Varying the two  $Y$ -shifts leads to a host of solutions. A number of these are shown in figure 6. The results show, among other properties, the need for blade 3 to be swung more than blade 2 in general to affect comparably the motion upstream, because of sheltering, cf. Glauert (1948). This ties in with the  $m^{1/6}$  incidence angles discussed below. Other comments analogous with those earlier for two blades hold here, while the associated lift and drag properties are considered in §5. A similar inverse procedure could be used for more blades.

Suppose now however that the number  $n$  of blades is large. An extension of the previous analysis for many blades would be expected to apply downstream under certain circumstances. As before there is a wide variety of configurations possible, but the following argument appears to cover many of interest. The characteristic viscous edge velocity  $V_\infty$  grows like  $m^{1/6}$  from (3.4b) and the corresponding viscous slopes in tier II there are also of order  $m^{1/6}$ , on the  $m$ th blade: see (3.7). Thus the typical viscous slopes are large downstream, and likewise for the viscous thicknesses. So for any fixed  $O(1)$  blade shapes and orientations the viscous displacements  $\delta_\pm$  are expected to dominate, implying that the symmetric-flow description of §3 for large  $n$  covers the current non-symmetric motions also, to leading order. The effect of non-symmetry is felt only at higher order, provoking a relative adjustment of order  $m^{-1/6}$  in each tier II far downstream.

The above is a prime result for many non-symmetric blades, independent of their shapes and orientations. To alter it the blade incidence for example would have to be proportional to  $m^{1/6}$  as the blade marker  $m$  increases downstream, unless something subtle arises from the summation over many blades. This option of  $m^{1/6}$  dependence in the blade configuration seems unrealistic at first sight, but in fact it could be of much value in pointing to what happens at angles of incidence greater than the present  $O(Re^{-1/2})$  values, and similarly for the blade thicknesses, cambers, etc. The matter is taken up in §6.

## 5. Lift and drag

Four integral properties to consider here are as follows:

$$A_m \equiv \int_{a_m}^{b_m} \{p_+(x, 0)f'_+(x) + p_-(x, 0)f'_-(x)\} dx, \quad (5.1)$$

$$B_m \equiv \int_{a_m}^{b_m} \{\tau_w^{(+)}(x) + \tau_w^{(-)}(x)\} dx, \quad (5.2)$$

$$C_m = \int_{a_m}^{b_m} \{p_-(x, 0) - p_+(x, 0)\} dx, \quad (5.3)$$

$$D_m \equiv \int_{a_m}^{b_m} \{\tau_w^{(+)}(x)f'_+(x) - \tau_w^{(-)}(x)f'_-(x)\} dx, \quad (5.4)$$

representing in turn the integrated pressure force in the streamwise direction, the integrated shear-stress contribution in the same direction, the integrated pressure force in the direction normal to the stream, and the integrated shear stress in the same direction. These are defined for the typical  $m$ th blade. A sign convention such that  $\tau_w^{(\pm)} > 0$  is taken, and as a reminder the blade upper and lower surfaces are  $y = \pm Re^{-1/2}f_{\pm}(x)$  respectively.

While all of (5.1)–(5.4) contribute partially to the lift and drag, however, the main ones are (5.2), (5.3). Indeed to leading order

$$[\text{drag, lift}] / \rho_D u_D^2 = Re^{-1/2} [B_m, C_m] \quad (5.5a, b)$$

per blade, whereas the  $A_m, D_m$  integral contributions arise only at order  $Re^{-1}$  approximately, as do leading-edge contributions from the local square-root response in the displacement and/or for rounded blade noses for example. Those leading-edge contributions are associated in the present context with the Navier–Stokes zone of streamwise and normal extent  $O(Re^{-1})$  at each blade nose wherein the pressure  $p$  becomes of order unity, comparable with the velocities  $u, v$  there, cf. Van Dyke (1964). The next-order terms in drag and lift come instead from the triple-deck behaviour near each trailing edge, yielding correction terms of order  $Re^{-7/8}$  to both (5.5a,b) in general, cf. Stewartson (1974), Brown & Stewartson (1975), Smith (1983). Also, the effects from both blade surfaces are included in (5.5a,b).

The values of the lift and drag are of interest for individual blades as well as for the total configuration. Sample values of  $B_m, C_m$  are given in figure 7. In the symmetric blade arrangement the lift part  $C_m$  is zero of course and the dominant drag part  $B_m$  represents a viscous influence alone (§3). On the other hand non-symmetric arrangements usually yield non-zero lift and drag parts, and both of these are combined viscous–inviscid influences because of the viscous–inviscid interactions

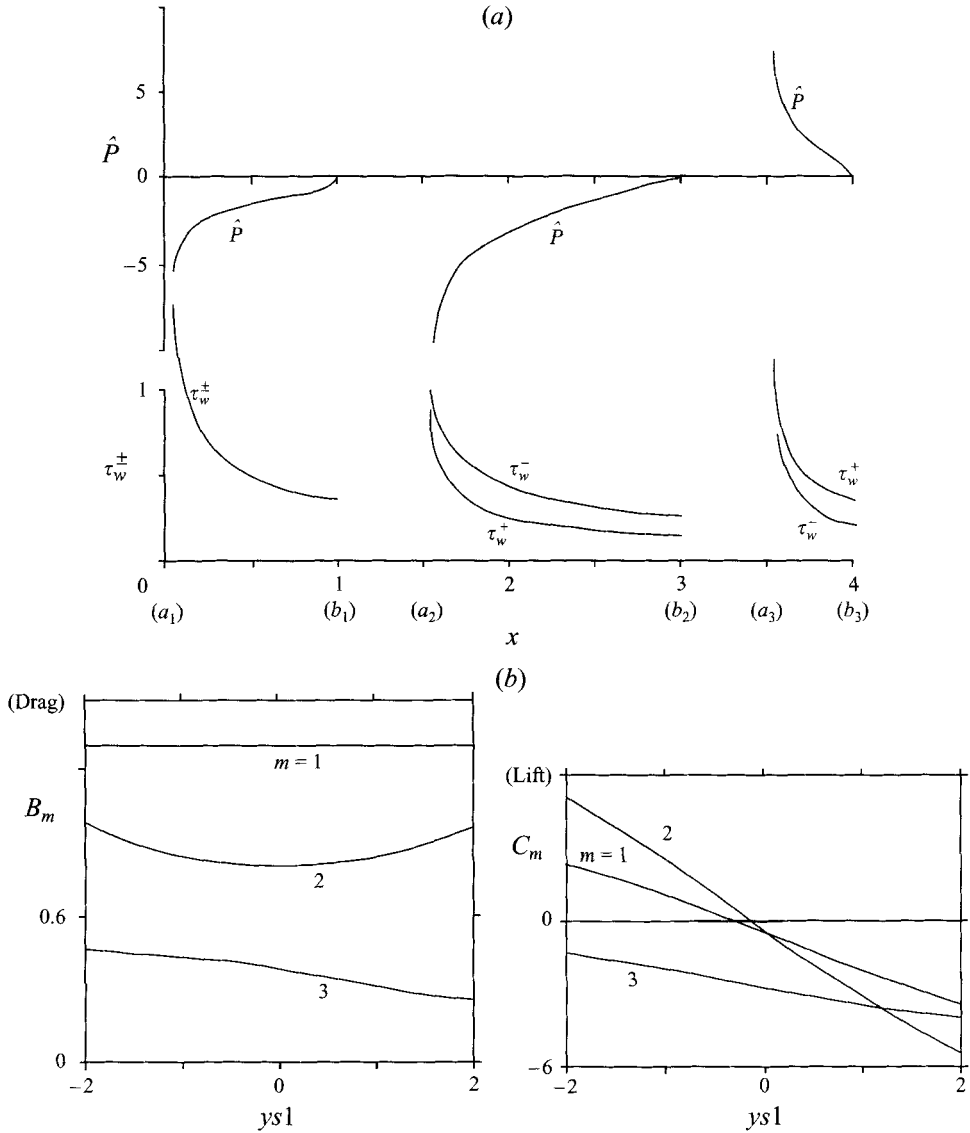


FIGURE 7. A sample plot of  $\tau_w^\pm, \hat{P}$  on blades 1-3 for a 3-bladed non-symmetric arrangement as in figure 6 when  $ys1 = -2, ys2 = 2$ ; the corresponding  $\alpha_2, \alpha_3$  values are given in the previous figure. Other blade arrangements can reverse some or all of the signs in  $\hat{P}$ , thus reversing the lift. (b) The drag and lift contributions ( $B_m, C_m$ ) for varying  $ysl$ , fixed  $ys2 = 2$ , showing various positive and negative lift contributions on the three blades. Note that the drag contribution on blade 1 stays uniform throughout.

present then (§4). On top of that, the results above show the sheltering effects on successive blades in the current, sequential, multi-blade arrangements, although the mean-value property (3.10) holding for both symmetric and non-symmetric many-blade configurations indicates that sheltering is limited as regards the drag, and there is an analogous limitation concerning the lift in view of the findings in the final two paragraphs of §4.

## 6. Further comments

This study has concentrated on blade-wake or airfoil-wake interactions for two-dimensional multiple-blade flows in symmetric and non-symmetric situations. The work has found or confirmed at least two new forms of interaction, and an account of another is given in the next paragraph. One of these interactions is for non-symmetric configurations, in §4, where the viscous boundary layers (and wakes) and the inviscid potential flow outside must be resolved simultaneously. A second interaction in non-symmetric or symmetric flows is associated with the many-blade case, in both §3 and §4, which shows a doubly viscous structure being produced in the normal direction and two length scales acting in the streamwise direction, as far as the downstream behaviour is concerned. The Blasius solution perhaps surprisingly applies 'in the mean' there. This can be so even if there is much more gap than blade, as in for example helicopter applications. A further significant feature is the computational scheme which is felt to be flexible as well as accurate, but we would tend to highlight the new interactions (above and below) equally. All of these interactions are peculiar to multi-blade flows and involve viscous combined with inviscid effects, in contrast with most previous approaches in the area.

The present two-dimensional theory and computations may also yield helpful ideas on the effects of non-symmetry in other settings. The interactions above in particular provide starting points for further studies. Likewise, the influences of unsteadiness and three-dimensionality are clearly of importance in reality as well as in theory. Further for the non-symmetric case, although it becomes increasingly difficult to handle numerically motions with more than a few blades (see §4), the many-blade analysis turns out to be useful again then, as described near the end of §4, suggesting that the symmetric and the non-symmetric cases provoke a common response far downstream. Let us explore that response a little further. An intriguing point is that in the inner viscous sublayer II on the  $m$ th blade the inertial force  $u\partial u/\partial x$  is reducing downstream like  $m^{-2/3}$  (since  $u \propto m^{-1/3}$  but the blade chord stays  $O(1)$ ), whereas the originally smaller outer pressure is growing in the form  $Re^{-1/2}m^{1/6}$ , being proportional to the slope of the displacement (added to the blade shape). So the pressure feedback will enter the reckoning in the sublayer momentum balance when  $m^{-2/3} \sim Re^{-1/2}m^{1/6}$ , giving  $m \sim Re^{3/5}$ . Hence a new stage occurs at a

$$\text{downstream distance} \sim Re^{3/5}, \quad (6.1)$$

since each blade has typical chord length of  $O(1)$ . Three scales then matter in the normal direction, namely

$$y \sim Re^{-2/5}, Re^{-1/5}, 1, \quad (6.2a-c)$$

where (6.2a) stems from (3.7) in the sublayer, (6.2b) is implied by (3.4a-c) in the core, and (6.2c) is from the outer potential flow, cf. (2.3)ff. The corresponding forms inferred for the streamwise velocity are

$$u = O(Re^{-1/5}), u_0 + O(Re^{-1/5}), 1 + O(Re^{-2/5}) \quad (6.3a-c)$$

from similar reasoning, while the pressure  $p$  is of order  $Re^{-2/5}$ . The new stage and scales implied here are almost exactly the same as in the triple-deck-like structure of Smith (1976) for internal flows, associated with the gradually reducing value of  $\lambda \propto m^{-1/2}$  downstream. The boundary-layer equations and constraints remain as in (3.8a-f) in effect but with the unknown pressure gradient  $-\partial p_1/\partial x$  added to the momentum equation,  $p_1$  being related to the unknown displacement which is effectively  $b$  in (3.9). This is nevertheless a novel interaction which is additional to

the inner-outer interaction of §§2.1 and 4 and which has a few unusual features, such as a triple-deck-like structure occurring in the absence of a continuous solid surface upstream and requiring a periodic-streamwise solution. We should re-emphasize that it is again peculiar to multi-blade motions and, perhaps most significantly, it covers the entirety of each blade and wake, as opposed to the usual single-airfoil interactions which are far more localized affairs. It should also allow regular separations and eddy closures to take place as the blade thickness, camber or incidence angle is increased, unlike in §§2–5 (where forward flow is usual), and that is of interest theoretically and practically. The comment in §4 on blade angles proportional to  $m^{1/6}$  also ties in with the scales of (6.1)–(6.3). Furthermore, under the conditions of (6.1)–(6.3) unsteadiness can make itself felt in the sublayer first, because the typical velocities are smaller there than elsewhere (see (6.3a)), whereas under the conditions of §§2–5 unsteadiness, in the sense of extra time derivatives appearing in the momentum equations, matters equally inside and outside the boundary layer. The time scales are given by

$$t \sim Re^{1/5}, \quad t \sim 1, \quad (6.4a, b)$$

respectively for (6.1)–(6.3) and for §§2–5, where  $t$  is based on  $\ell_D u_D^{-1}$ . A robust numerical scheme perhaps of the kind developed in §§3 and 4 could be useful in this new context of (6.1)–(6.4) also.

Many additional matters follow from the above. First, only laminar steady flows have been studied so far, but a start on unsteady effects leading on to transition for example can be made via the time scales in (6.4a,b). Various paths of transition are likely to arise depending on the input frequencies and disturbance amplitudes, for example Tollmien–Schlichting type, inflectional type and relatively-high-frequency type (results for the latter were obtained by Professor O.R. Burggraf and F.T.S. in 1983 with regard to trailing-edge flows). Second is the question of whether an interactive structure similar to that in (6.1)–(6.3) holds also in the three-dimensional rotating-flow setting discussed in §§1, and 2.3 and Smith & Timoshin (1996). After all, flow structures analogous with those of §§2–5 do hold in that setting. The structure of (6.1)–(6.3) or (6.4) when extended to three dimensions may well allow blade-tip flows and associated separations/shedding to be included. There is potential application moreover to flows over two-dimensional or three-dimensional arrays of buildings, or even cities, with short-scale periodicity or randomness within the larger-scale motion. Third, there are allied issues such as slip-streaming and the possible benefits with regard to sheltering, as in the local velocity reductions (cf. §§3 and 4) and the lift and drag (cf. §5) when the number  $n$  of blades is increased. Connected with this are the various contributions to lift and drag on the whole multi-blade system or on individual blades/airfoils in the system. Some features of sheltering are covered already by classical inviscid theory, e.g. Glauert (1948), but the current work has added the effects of viscosity and associated vorticity shedding. Fourth, the many-blade analysis seems to be relevant to fairly moderate values of  $n$  in Smith & Timoshin (1996) and the same applies in this work. Fifth, an interesting point arose from discussions with Professor S.I. Chernyshenko, after this work. In the current sequential setting the whole blade system stays essentially immersed in successive boundary layers, as the intersections of vorticity wakes with blades persist downstream. Thus in a sense the global angle of incidence remains zero for the complete blade system even though individual blade angles may be non-zero (§4). For some other real configurations however non-zero global angles are relevant, this corresponding for instance to a growing shift in  $Y$  of successive blades downstream by an amount proportional to  $m$ , in the theory of §4. That gives an interesting configuration, not least because of

the importance attached earlier to  $m^{1/6}$  growth. Growth larger than  $m^{1/6}$  reduces the viscous vorticity-sheltering effect downstream, as well as reducing the ability to handle global separations rationally as in (6.1)–(6.4). Further studies could be worthwhile for non-zero global angles, involving turning of the original free-stream flow. Sixth, further investigation is also called for on the matter of whether the presence of multiple blades reduces the likelihood of separation and transition, or not, and here again the stage (6.1)–(6.4) could be enlightening. In that sense the interaction of (6.1)–(6.4) is perhaps the most significant of the viscous–inviscid interactions found in this study, allowing the complete blade–wake configuration to be accommodated even with separations arising. Finally, there are related questions concerning flows past blades positioned in parallel or overlapping rather than in sequence as here.

Thanks are due to ESPRC for computing facilities, to Professor S.I. Chernyshenko for helpful discussions, to the referees for their comments, and to personnel at Westland Helicopters, DRA Farnborough and Kenwood UK for their interest.

## REFERENCES

- BROWN, S. N. & STEWARTSON, K. 1970 *J. Fluid Mech.* **42**, 561–584.  
 BROWN, S. N. & STEWARTSON, K. 1975 *Aero. Q.*, Nov., 275–280.  
 DAVIS, S. S. & CHANG, I.-C. 1986 Invited survey paper, *AIAA 24th Aerosp. Sci. Mtg.*, Jan. 6–9 Reno, Nevada, USA. Paper 86–0336.  
 GLAUERT, H. 1948 *The Elements of Aerofoil and Airscrew Theory*, 2nd edition. Cambridge University Press.  
 GOLDSTEIN, S. 1930 *Proc. Camb. Phil. Soc.* **26**, 1–30.  
 HAWKINGS, D. L. & LOWSON, M. V. 1974 *J. Sound Vib.* **36**, 1–20.  
 MESSITER, A. F. & STEWARTSON, K. 1972 *AIAA J.* **10**, 719.  
 MOORE, D. W. & SAFFMAN, P. G. 1973 *Proc. R. Soc. Lond. A* **333**, 491–508.  
 MUSKHELISHVILI, N. I. 1946 *Singular Integral Equations*. P. Noordhoff (English transl. 1953).  
 PARRY, A. B. & CRIGHTON, D. G. 1989 *AIAA J.* **27**, 1184–1190.  
 RILEY, N. 1996 *Handbook of Acoustics*, chap. 30. Wiley.  
 SEDDON, J. 1990 *Basic Helicopter Dynamics*, BSP Professional Books. Oxford.  
 SMITH, F. T. 1976 *J. Fluid Mech.* **78**, 709–736.  
 SMITH, F. T. 1983 *J. Fluid Mech.* **131**, 219–249.  
 SMITH, F. T. & TIMOSHIN, S. N. 1996 *Proc. R. Soc. Lond. A* **452**, 1301–1329.  
 SPENCE, D. A. 1970 *J. Fluid Mech.* **44**, 625–636.  
 STEWARTSON, K. 1974 *Adv. Appl. Mech.* **14**, 145.  
 VAN DYKE, M. 1964 *Perturbation Methods in Fluid Mechanics*. Academic Press.  
 WAKE, B. E. & BAEDER, J. D. 1994 *Am. Helicopter Soc. Aeromech. Specialists Conf.*, San Francisco, CA, USA, Jan. 19–21.